

Review

Antimony (Sb)-Based Anodes for Lithium–Ion Batteries: Recent Advances

Sreejesh Moolayadukkam ^{1,*}, Kaveramma Appachettolanda Bopaiiah ¹, Priyanka Karathan Parakkandy ² and Siby Thomas ^{3,*}

¹ Centre for Nano and Soft Matter Sciences (CeNS), Arkavathi, Survey No. 7, Shivanapura, Dasanapura Hobli, Bengaluru 562162, India; kaveramma990@gmail.com

² Department of Physics, M. S. Ramaiah University of Applied Sciences, Bengaluru 560058, India; kppriyanka19@gmail.com

³ Department of Electrical and Computer Engineering, Technical University of Munich (TUM), Karlstrasse 45-47, 80333 Munich, Germany

* Correspondence: sreejeshmnasc@gmail.com (S.M.); siby.thomas@tum.de (S.T.)

Abstract: To mitigate the use of fossil fuels and maintain a clean and sustainable environment, electrochemical energy storage systems are receiving great deal of attention, especially rechargeable batteries. This is also associated with the growing demand for electric vehicles, which urged the automotive industries to explore the capacities of new materials for use in lithium–ion batteries (LIBs). Graphite is still employed as an anode in large majority of currently available commercial LIBs preserving their better cyclic stability despite enormous research efforts to identify viable alternatives with improved power and energy density. From this point of view, antimony acts as a promising material because it has good theoretical capacity, high volumetric capacity, good reactivity with lithium and good electronic conductivities. Recently, there have been many works that focused on the development of antimony as an alternative anode. This review tries to give a bird’s eye view comprising the experimental and theoretical insights on the developments in the direction of using antimony and antimony composites as anodes for rechargeable Li.

Keywords: Li–ion batteries; antimony; nanocomposites; capacity; density functional theory



Citation: Moolayadukkam, S.; Bopaiiah, K.A.; Parakkandy, P.K.; Thomas, S. Antimony (Sb)-Based Anodes for Lithium–Ion Batteries: Recent Advances. *Condens. Matter* **2022**, *7*, 27. <https://doi.org/10.3390/condmat7010027>

Academic Editor: Bernardo Barbiellini

Received: 16 January 2022

Accepted: 3 March 2022

Published: 5 March 2022

Publisher’s Note: MDPI stays neutral with regard to jurisdictional claims in published maps and institutional affiliations.



Copyright: © 2022 by the authors. Licensee MDPI, Basel, Switzerland. This article is an open access article distributed under the terms and conditions of the Creative Commons Attribution (CC BY) license (<https://creativecommons.org/licenses/by/4.0/>).

1. Introduction

Lithium–ion batteries have become a part of our day-to-day life in the past few years, and it is difficult to imagine a field where they are not used much. High energy and power density, excellent cycling stability and high operating voltages are the properties of existing lithium–ion batteries. The mechanisms behind these properties are mainly determined by the cathodes and anodes as well as the transport of electrons and ions through the electrolyte through separator. Hence, for further improvements in fields such as electric vehicles, it is required to improve these properties [1–3]. Currently, graphite is the most used anode material, with a theoretical capacity of 372 mAh g^{−1}; it has been shown to have excellent cycling stabilities and moderate specific capacitance [4]. However, the current developments in the field of electric vehicles and other smart electronic gadgets require better batteries. Because of this reason, the scientific community is in search of a better material that can replace graphite with a higher-capacity anode. The alloying mechanism usually favors higher capacities compared to the one involved in graphite, but usually involves high volume changes during the reaction, which results in poor electrode stability and cyclic life [5]. Silicon is one of the most promising alloying anodes with very high theoretical capacity (4200 mAh g^{−1}), but it lacks stability due to its associated high volumetric changes (400%) [6] during the intercalation/deintercalation of lithium. Another alloying anode of importance is Tin, which has a higher capacity of 990 mAh g^{−1} corresponding to the formation of Li₂₂Sn₅ phase. The associated 250+% change in the

volume means it is difficult to stabilize the electrode [7]. Alloying anodes with lesser structural changes would be an alternative to silicon from this point of view. Among these alloying electrodes, antimony (Sb) has relatively lower volume expansion (135%), good chemical properties, a thermal stability similar to Si and Sn, and Li^+ insertion capacity of 660 mAh g^{-1} (Li_3Sb) [8]. An antimony electrode has a puckered layered structure which enables it to exhibit high conductivity and reactivity, and reversibility at a moderate current density. Sb also shows a very high volumetric capacity of 1890 Ah L^{-1} , which is equivalent to that of Si and 2.5 times higher than the commercially used graphite anodes [8]. These exciting properties of antimony have garnered great attention from the scientific community in search of alternative anodes with enhanced performance. Figure 1 represents a graphical representation of year-wise number of publications related to Sb anodes in lithium-ion batteries.

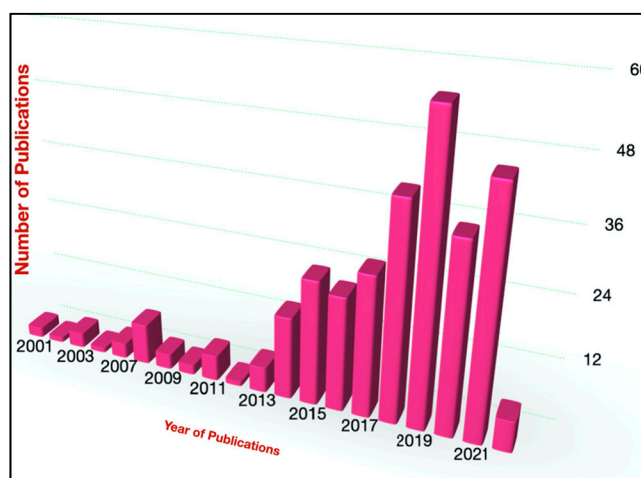


Figure 1. Graphical representation of year-wise number of scientific publications related to lithium-ion storage antimony anodes (Web of Science statistics).

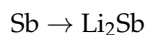
Safety is one of the major concerns in LIBs which has to be given highest priority while designing batteries for specific applications. Applications such as electric vehicles use battery packs containing a large number of individual cells put together, and any faulty battery can cause large-scale explosions [2]. Sb is a better alternative in this regard than the typically utilized graphite anodes. Dendrite creation is much more likely due to graphite's potential against Li/L^+ and electrolyte breakdown, as well as the development of SEI. As a result, kinetics are sluggish, and safety is an issue [9]. Another reason for looking into other Sb anodes is the observed incompatibility of graphite with certain high-performance electrolytes (such as propylene carbonate) and high-performance cathodes (such as Mn-containing spinels) [10].

In view of the commercial applications, despite the higher capacity of antimony compared to the traditionally used graphite anodes, the cyclic stabilities are not on par and this bottleneck has to be resolved for the commercialization. There have been many efforts to engineer the micro- and nanostructures of the antimony anodes and improve the cyclic stabilities by accommodating volume change during cycling. Making composites with materials of high porosity to accommodate the stress and strain is also a routinely used method. This review focuses on antimony and antimony-based nanostructures and heterostructures and explained their potential as anodes by nanoengineering and composite formation.

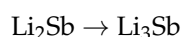
2. Mechanism of Lithium-Ion Storage in Sb Anodes

These lithium-ions are stored inside Sb-based anodes through an alloying reaction. The mechanism involved is well discussed by many authors. Chang et al. reported that the lithium insertion and extraction follows different pathways. Three distinctive phases (Sb,

Li_2Sb and Li_3Sb) are reported in a Li and Sb alloy [11,12]. The Sb exist in the rhombohedral structure, Li_2Sb is hexagonal and Li_3Sb is cubic. The charge and discharge mechanism involved is depicted in Figure 2. During the discharge process, the incoming Li-ions interact with Sb and form Li_2Sb . This phase transformation is well studied in the literature.

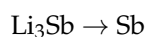


This phase undergoes further transformation to form Li_3Sb .



Li_3Sb formed during this step is a high temperature polymorph usually observed only at temperatures above 650 °C ($\beta\text{-Li}_3\text{Sb}$) [13].

During the charge process Li_3Sb directly converts to Sb without undergoing a transformation to the intermediated Li_2Sb [8,14].



Similar systems such as sodium-ion batteries do not follow the same pathway, and the importance of this difference is not well described in the literature. There has been significant effort to use Sb as an anode for sodium and potassium ion batteries. Though it is fundamentally interesting to study these systems, the very high-volume changes associated with these systems (390% for Na, 407% for K) make it difficult to stabilize the electrodes and must be addressed accordingly [15].

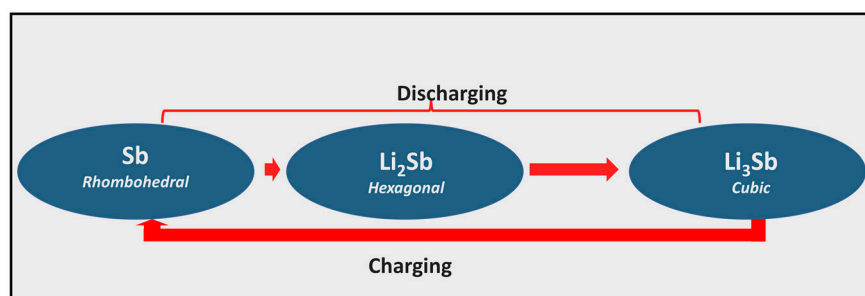


Figure 2. Charge–discharge mechanism in an Sb battery.

3. Recent Developments

He et al. reviewed the developments in the field up to 2018 and this review primarily focused on developments after this period [8]. Initially, the research focused on developing Sb-based anodes by changing the micro- and nanostructuring to accommodate the volume changes. The majority of these earlier work fall into the following categories:

1. **Hollow nanostructured materials:** Materials with an interior space easily can accommodate the volume changes and these kinds of materials are synthesized to utilize this aspect. Additionally, the nano sizing would usually give rise to the short paths for electron mobilities which can improve performance of the material. The most-reported hollow structures are synthesized using the templating method, but better methods for synthesis of such structures are urgently needed.
2. **Nanorods:** Nanorods are a very common structure used in silicon anodes to accommodate the volume changes associated with them. These structures also allow the electrolytes and electrons to be percolated easily. The hydrothermal method, electrodeposition or chemical vapor deposition techniques are the commonly used methods for nanorod synthesis.
3. **Two-dimensional (2D) structures:** These structures are designed to provide high electrical conductivity and to increase the energy density. The interlayer spacing

present in the antimony anodes not only improves the lithium-ion storage but also helps to achieve fast ion transport with a small ionic radius.

4. **Nanoporous structures:** Nanostructured porous materials are found to be effective in reducing the strain which occurs due to volumetric changes. They aim to maintain constant stability in the electrode and improve the kinetics of the material, thereby accelerating the ion transport and improving the cyclic and rate capabilities. The anode materials in this morphology are easy to construct using de-alloying low-cost steps and the morphology is controlled with the Sb material. The nanostructuring of the material had improved the performance of Sb anodes in several aspects, but failed to meet the industry standards used in commercial devices. Keeping this in mind, developments after 2018 focused on composites mainly using carbon additives.

To accommodate the volume changes, research on hollow nanospheres of Sb, which shows better stability and good capacities, was searched for in the literature [17]. However, synthesis methods for such nanostructures are tedious, time-consuming and less efficient. Boebinger et al. tackled this issue by utilizing the in situ formation of hollow space during charge–discharge cycling. They discussed hollow structure formation and the stabilization of antimony anodes during cycling in detail. They found that the nanocrystals should have a particular size (~15 nm) and a protective layer of oxides to unleash the complete potential of antimony. In situ studies show the formation of voids during the initial cycling and subsequent filling of lithium in the cycles followed [18]. The void spaces created during this process was permanent and acted like any other ex situ-prepared hollow nanostructures. By doing this, they could show that Sb batteries can be cycled up to 100 cycles with high stability. The formation of such structures during cycling is not well discussed in the literature and could have the potential to be developed as a method for improving the performance of antimony anodes. Apart from in situ methods, special synthesis protocols also could produce nanostructures that can effectively handle the volume changes. Three-dimensional antimony nano chains are reported to have good performance in absorbing the stress and strain induced due to lithiation and delithiation. Rodriguez et al. used a two-stage process involving the reduction of Sb salt for the formation of Sb nanoparticles followed by a capping process to obtain Sb nano chains. This synthesis resulted in well-ordered nanoparticles with a size ~30 nm (see Figure 3a–c). Through electrochemical studies, they have shown that (see Figure 3d–e) the material can perform well up to 100 cycles with limited capacity fading. This is attributed to the nanochain structure which could effectively hold the electrode material during cycling. Electrode fabrication also plays a key role in stabilizing the anode performance. Wang et al. approached the problem by modifying the electrode fabrication using polyimide additives. The interaction between polyimide and the binder carboxymethyl cellulose could hold the electrode material (Sb microparticles) intact with the current collector. This strategy also helped in obtaining stability for up to 100 cycles and performed well even at high rates of charge and discharge [19]. These methods could be clubbed together to obtain synergetic enhancement in the performance of Sb anodes in the future.

To handle the volumetric changes, Sb nanoparticles can also be inserted inside porous conducting materials which could minimize the stress and strain during cycling. Yi et al. reported a strategy for synthesizing Sb incorporated carbon Sb/C systematically starting from ZIF-67. Carbonization reaction converts ZIF-67 to Co/C composites, as shown in the TEM images in Figure 4a,b. A replacement reaction is followed to obtain Sb/C composites. These kinds of reactions could be a reliable route to synthesize nanoparticles inside porous matrices. It is reported that (in Figure 4c) the large initial capacity loss is due to the SEI formation during the first discharge but maintains high capacity for up to 500 cycles (see Figure 4e). This high stability, along with good rate capabilities up to 5 C (see Figure 4d), could be useful for commercial applications [20]. Apart from ease of synthesis, economic viability should also be the focal point of research. From this point of view, Wang et al. reported a method wherein a chemical route is used to obtain the Sb nanoparticles inside porous carbon structures [21]. However, the cyclic life reported was inferior compared to

the earlier result. This tradeoff between viable synthesis and anode performance has to be addressed to progress the antimony anode technology to the next level. Table 1 summarizes recent developments in the antimony anodes and it can be clearly seen that there should be efforts to improve the cyclic life as well as the rate capabilities.

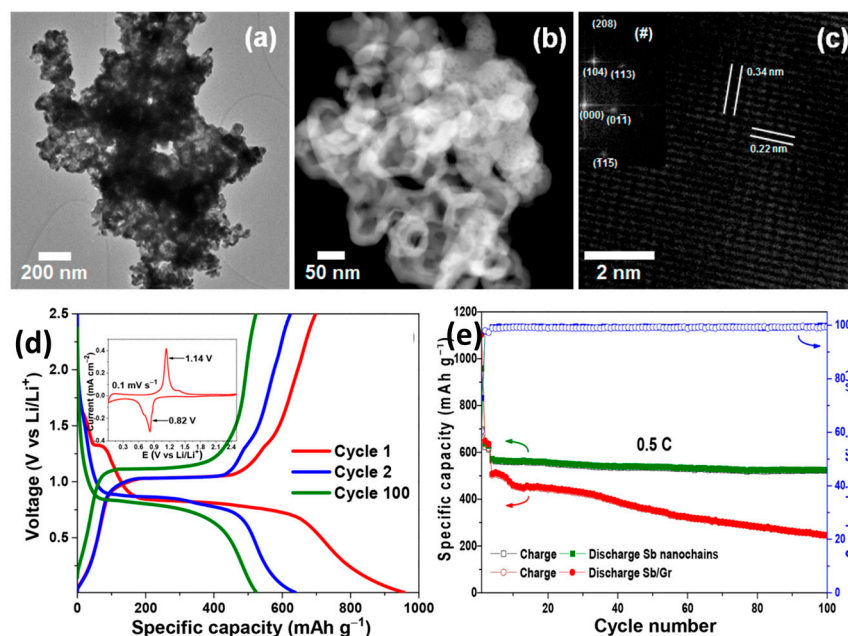


Figure 3. (a–c) TEM images (d) galvanostatic charge–discharge characteristics along with CV (inset) and (e) cyclic stability studies of Sb nano chains. Reprinted (adapted) with permission from [16]. Copyright 2019, American Chemical Society.

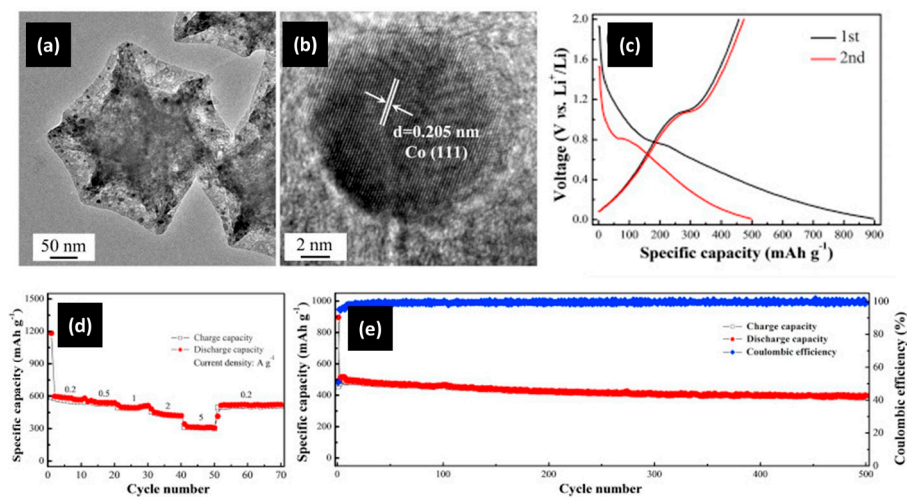


Figure 4. (a,b) ZIF converted Co/C composite (c) initial charge–discharge, (d) rate capabilities and (e) cycling of Sb/C anodes. Reprinted with permission from Ref. [20]. Copyright 2020, Elsevier.

Table 1. The table summarizes the recent developments in the antimony anodes for lithium-ion batteries.

| No. | Material/Details | Capacity | Rate Capability | Cyclic Stability | Residual Capacity | Refs. |
|-----|---|--|---|--|----------------------------|-------|
| 1 | Sb-carbon nanocomposite | 550 mAh g ⁻¹ @ 230 mA g ⁻¹ | 400 mAh g ⁻¹ @ 1.15 A g ⁻¹ | 250 cycles at a current rate of 230 mA g ⁻¹ | 400 mAh g ⁻¹ | [22] |
| 2 | Electrophoretic deposited antimony/reduced graphite oxide | 731 mAh g ⁻¹ @ 0.1 Ag ⁻¹ | 498.1 mAh g ⁻¹ @ 0.5 Ag ⁻¹ | 100 cycles @ 0.5 A g ⁻¹ | ~370.1 mAh g ⁻¹ | [23] |
| 3 | Sb nanoparticles encapsulated into porous carbon matrix | 582.7 mAh g ⁻¹ @ 0.2 A g ⁻¹ | 437.1 and 315.4 mAh g ⁻¹ @ 2 and 5 A g ⁻¹ | 70 cycles @ 0.2 A g ⁻¹ | 400.6 mAh g ⁻¹ | [20] |
| 4 | Metallic Sb nanoparticles embedded in carbon nanosheets | 597.8 mAh g ⁻¹ @ 200 mA g ⁻¹ | 418 mAh g ⁻¹ @ 5.0 A g ⁻¹ | 100 cycles @ 200 mA g ⁻¹ | 230 mAh g ⁻¹ | [24] |
| 5 | Nanostructured antimony/carbon composite | 451.2 mAh g ⁻¹ @ 100 mA g ⁻¹ | 149.8 mAh g ⁻¹ @ 1600 mA g ⁻¹ | 50 cycles @ 1600 mA hg ⁻¹ | 131.6 mAh g ⁻¹ | [25] |
| 6 | Sb nanoparticles encapsulated in 3D porous carbon for lithium-ion and potassium-ion batteries | 1224.9 mAh g ⁻¹ @ 100 mA g ⁻¹ . | 387.2 mAh g ⁻¹ @ 2 A g ⁻¹ | 55 cycles @ 0.5 A g ⁻¹ | 90 mAh g ⁻¹ | [21] |
| 7 | Nanostructured carbon/antimony composites | 354.4 mAh g ⁻¹ @ 1000 mAh g ⁻¹ . | 470.4 mAh g ⁻¹ @ 100 mA g ⁻¹ | 200 cycles @ 100 mA g ⁻¹ | 323.4 mAh g ⁻¹ | [26] |
| 8 | Sb@C/expanded graphite | 486 mAh g ⁻¹ @ 1.0 A g ⁻¹ | 287 mAh g ⁻¹ @ 2.0 A g ⁻¹ | 600 cycles @ 1.0 A g ⁻¹ | 274 mAh g ⁻¹ | [27] |
| 9 | Sb-coated mesophase graphite powder | 329 mAh g ⁻¹ @ 0.325 mA cm ⁻² | 329 mAh g ⁻¹ @ 0.325 mA cm ⁻² | 20 cycles @ 0.325 mA cm ⁻² | 101.23 mAh g ⁻¹ | [28] |
| 10 | The nanocomposites of carbon nanotube with Sb and SnSb0.5 | 822 mAh g ⁻¹ @ 50 mA g ⁻¹ | 200 mAh g ⁻¹ @ 50 mA g ⁻¹ | 50 cycles @ 50 mA g ⁻¹ | 147 mAh g ⁻¹ | [29] |
| 11 | One-dimensional Sb@TiO ₂ composites | 752.2 mAh g ⁻¹ @ 100 mA g ⁻¹ (3 C) | 450.2 mAh g ⁻¹ @ 100 mA g ⁻¹ | 100 cycles @ 100 mA g ⁻¹ | 340.2 mAh g ⁻¹ | [30] |
| 12 | Polyimide-cellulose interaction with Sb particle and binder | 580 mAh g ⁻¹ is obtained at 1 A g ⁻¹ | 380 mAh g ⁻¹ @ 20 C (13.2 A g ⁻¹), | 100 cycles @ 13.2 A g ⁻¹ | 270 mAh g ⁻¹ | [19] |
| 13 | Strongly binding natural stibnite on carbon fiber as anode for lithium-ion batteries | 669.6 mAh g ⁻¹ @ 1.0 A g ⁻¹ | 264.1 mAh g ⁻¹ @ 5 A g ⁻¹ | 100 cycles @ 5 A g ⁻¹ | 230 mAh g ⁻¹ | [31] |
| 14 | Scalable synthesis of Sb/MoS ₂ /C composite | 763 mAh g ⁻¹ @ 0.2 A g ⁻¹ | 459 mA h g ⁻¹ @ 5.0 A g ⁻¹ | 250 cycles @ 5.0 A g ⁻¹ | 161 mAh g ⁻¹ | [32] |
| 15 | Three-dimensional cross-linked MnO/Sb hybrid nanowires co-embedded nitrogen-doped carbon nano tubes | 592 mAh g ⁻¹ @ 1 A g ⁻¹ | 217 mAh g ⁻¹ @ 10 A g ⁻¹ | 1100 cycles @ 10 A g ⁻¹ | 124 mAh g ⁻¹ | [33] |
| 16 | Microsized antimony as a stable anode in fluoroethylene carbonate containing electrolytes | 689 mAh g ⁻¹ @ 5000 mA g ⁻¹ | 648 mAh g ⁻¹ @ 200 mA g ⁻¹ | 300 cycles @ 200 mA g ⁻¹ | 540 mAh g ⁻¹ | [34] |
| 17 | Three-dimensional antimony nanochains | 956 mAh g ⁻¹ @ 0.05 C | 523 mAh g ⁻¹ @ 0.5 C | 100 cycles @ 0.5 C | 430 mAh g ⁻¹ | [16] |
| 18 | Aerosol assisted synthesis of spherical Sb/C composites | 726 mAh g ⁻¹ @ 50 mA g ⁻¹ | 416 mAh g ⁻¹ @ 600 mA g ⁻¹ . | 150 cycles @ 100 mA g ⁻¹ . | 413 mAh g ⁻¹ | [35] |
| 19 | Controllable synthesis of Sb/reduced graphene oxide nanocomposite by oxygen-containing groups for ultra-stable lithium/sodium storage | 390.9 mAh g ⁻¹ @ 200 mA g ⁻¹ | 205.3 mAh g ⁻¹ @ 2000 mA g ⁻¹ | 1000 cycles @ 2000 mA g ⁻¹ | 100 mAh g ⁻¹ | [36] |
| 20 | Sodium/lithium storage behavior of antimony hollow nanospheres | 627.3 mAh g ⁻¹ @ 100 mAh g ⁻¹ | 435.6 mAh g ⁻¹ @ 1600 mA g ⁻¹ | 50 cycles @ 1600 mA g ⁻¹ | 435.6 mAh g ⁻¹ | [17] |

Table 1. Cont.

| No. | Material/Details | Capacity | Rate Capability | Cyclic Stability | Residual Capacity | Refs. |
|-----|---|--|---|-------------------------------------|----------------------------|-------|
| 21 | Sb nanoparticles encapsulated in 3D porous carbon as anode material for lithium-ion and potassium-ion batteries | 758.3 mAh g ⁻¹ @ 0.1 Ag ⁻¹ | 387.2 mAh g ⁻¹ @ 2 Ag ⁻¹ | 500 cycles @ 2 Ag ⁻¹ | 200 mAh g ⁻¹ | [21] |
| 22 | In situ synthesis of microspherical Sb@C composite anode with high tap density for lithium/sodium-ion batteries | 626.4 mAh g ⁻¹ @ 100 mA g ⁻¹ | 336.8 mAh g ⁻¹ @ 500 mA g ⁻¹ | 500 cycles @ 500 mA g ⁻¹ | 280 mAh g ⁻¹ | [37] |
| 23 | Highly efficient and stable Bi and Sb anodes using lithium borohydride as solid electrolyte in Li-ion batteries | 4393.4 mAh cm ⁻³ (657.7 mAh g ⁻¹) | 4148.3 mAh cm ⁻³ @ 621 mAh g ⁻¹ | 50 cycles @ 621 mAh g ⁻¹ | 150 mAh g ⁻¹ | [38] |
| 24 | Electrodeposition of Sb/CNT composite films | 750 mAhg ⁻¹ @ 0.1 mA g ⁻¹ | 450 mAhg ⁻¹ @ 0.1 mA g ⁻¹ | 100 cycles @ 0.1 mA g ⁻¹ | 200 mAh g ⁻¹ | [39] |
| 25 | Spontaneous and reversible hollowing of alloy anode nanocrystals for stable battery cycling | 800 mAh g ⁻¹ @ 660 mA g ⁻¹ | 200 mAh g ⁻¹ @ 660 mA g ⁻¹ | 100 cycles @ 660 mA g ⁻¹ | 200 mAh g ⁻¹ | [18] |
| 26 | Electrophoretic deposition of antimony/reduced graphite oxide hybrid nanostructure | 370.1 mAh g ⁻¹ @ 0.5 Ag ⁻¹ | 128.7 mAh g ⁻¹ @ 4 A g ⁻¹ . | 100 cycles @ 4 A g ⁻¹ . | ~23.8 mAh g ⁻¹ | [23] |
| 27 | Sb nanoparticles anchored on reduced graphene oxides | 797.5 mAh g ⁻¹ @ 80 mA g ⁻¹ | 562.9 mAh g ⁻¹ @ 430 mA g ⁻¹ | 200 cycles @ 80 mA g ⁻¹ | 83.2 mAh g ⁻¹ | [40] |
| 28 | Reversible formation of networked porous Sb nanoparticles during cycling: Sb nanoparticles encapsulated in a nitrogen-doped carbon matrix with nanorod structures | 654 mAh g ⁻¹ @ 100 mA g ⁻¹ | 444.2 mAh g ⁻¹ @ 5000 mA g ⁻¹ | 500 cycles @ 100 mA g ⁻¹ | ~300.3 mAh g ⁻¹ | [41] |
| 29 | Facile citrate gel synthesis of antimony-carbon nosponge | 634.4 mAh g ⁻¹ @ 0.1 C | 405.97 mAhg ⁻¹ @ 10 C | 100 cycles @ 10 C | 153.1 mA h g ⁻¹ | [42] |
| 30 | Tailoring natural layered β-phase antimony into few layer antimonene | 488 mAh g ⁻¹ @ 5 C | 410 mAhg ⁻¹ @ 10 C | 40 cycles @ 10 C | 148 mAh g ⁻¹ | [43] |
| 31 | Ultrafine antimony (Sb) nanoparticles encapsulated into a carbon microfiber framework | 622 mAh g ⁻¹ @ 0.5 A g ⁻¹ | 507 mAh g ⁻¹ @ 2 Ag ⁻¹ | 5000 cycles @ 2 Ag ⁻¹ | 350 mAh g ⁻¹ | [44] |
| 32 | Porous Sb with three-dimensional Sb-nanodendrites | 651.6 mAh g ⁻¹ @ 0.05 A g ⁻¹ | 557.8 mAh g ⁻¹ @ 0.1 A g ⁻¹ | 110 cycles @ 0.1 Ag ⁻¹ | 532 mAh g ⁻¹ | [45] |
| 33 | Ion-assisted construction of Sb/N-doped graphene | 615 mAh g ⁻¹ @ 0.1 Ag ⁻¹ | 300 mAh g ⁻¹ @ 2 A g ⁻¹ | 200 cycles @ 2 Ag ⁻¹ | 240 mAh g ⁻¹ | [46] |
| 34 | Binder-free electrophoretic deposition of Sb/rGO on Cu foil | 370 mAh g ⁻¹ @ 1 C | ~170 mAh g ⁻¹ @ 4 C | 100 cycles @ 4 C | ~170 mAh g ⁻¹ | [47] |
| 35 | Synthesis and electrochemical properties of Pb/Sb@C composite for lithium-ion battery application | 600 mAh g ⁻¹ @ 0.2 C | 463 mAh g ⁻¹ @ 10 C | 100 cycles @ 10 C | 380 mAh g ⁻¹ | [12] |

Most of the works on Sb anodes focused on studying the performance in half cell assemblies. To evaluate the actual usability in real-life applications, it is also essential to check them in full-cell configurations. Zhan et al. explored the possibilities of using the electrodes in full cell assembly using metallic Sb nanoparticle embedded carbon nanosheets. The battery was fabricated in a configuration of Sb@C nanosheets || LiFePO₄/C and tested in between a potential window of 1.0 and 3.2 V. The first three charge cycle cycles are shown in Figure 5a, which shows two plateaus around 2.6 and 2.4 V. In full cell configuration, the material shows excellent cycling stabilities indicating the practical usage in lithium-ion batteries [24]. Similarly, Wang et al. reported Sb@TiO_{2-x} full cells against LiCoO₂ cathodes with good cycling stabilities [48]. In another report, Yu et al. described the fabrication of full cell using tiny pieces of Sb encapsulated in MOFs-derived carbon and TiO₂ hollow nanotubes [49]. The good performance and stabilities offered by Sb-based materials in full

cell configuration suggest that there is enough room to exploit the use of Sb for commercial applications.

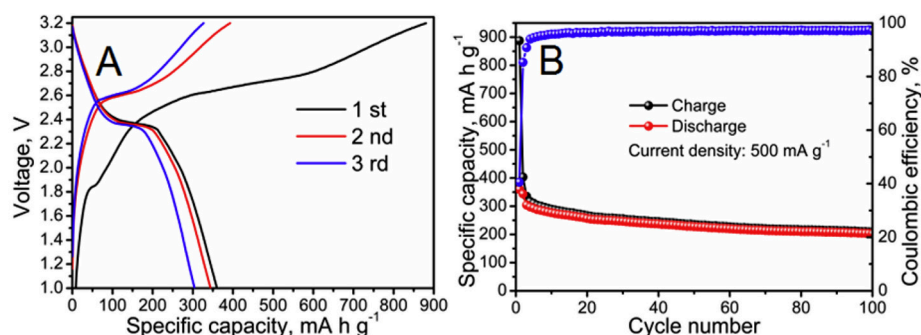


Figure 5. The electrochemical properties of the constructed Sb@C nanosheets || LiFePO₄/C full cell showing (A) cycling time at 500 mA g⁻¹ and (B) the first three charge/discharge curves at 500 mA g⁻¹. (Reproduced with permission from Ref. [24]. Copyright 2018, Elsevier.).

Safety is another important parameter to be considered while anodes are used in full cells. The electrode reactions and thermal runaways are the primary cause for fire in batteries. Manthiram group has carried out extensive studies on this aspect on Sb and Sb alloy-based anodes. Graphite, which is used in most of the commercial batteries, tends to have more SEI formed on the surface along with chances for dendrite formation. They found that, at 150° Celsius, the heat generation per unit capacity for both Sb and Cu₂Sb is 37% lower than graphite, which is a key region for preventing thermal runaway [50]. This study also suggests that the safety concerns of lithium-ion batteries can be greatly solved by using Sb in its anodes. Irrespective of its exciting properties, Sb is not an earth-abundant material. An antimony circular economy must be developed for successful use in battery technology. For this, the recovery of used antimony from batteries is going to be critical and there is no literature available on this.

4. Theoretical Studies on Sb and Sb-Based Nanostructures

In addition to experimental efforts to synthesize Sb-based anodes for LIBs, theoretical studies have also been carried out to understand the Li adsorption and storage properties of nanomaterials composed of Sb. Due to the widespread enthusiasm for and interest in 2D materials, different groups have reported the potential LIB applications of monolayer antimony (antimonene). In 2017, with the help of dispersion-corrected density functional theory calculations, Sengupta et al. compared the performance of free-standing monolayer Sb for Li and Na ion battery anode applications [43]. From their studies, they reported that although Na adsorption is superior compared to Li adsorption, the fully lithiated configuration (LiSb) possess a capacity of 208 mAh g⁻¹ with an average open-circuit voltage of 2 V. They also reported a low energy barrier of 0.38 eV for the diffusion of Li atoms on monolayer Sb.

Later, in 2018, Su et al. carried out density functional theory (DFT) studies using the Vienna ab-Initio Simulation Package (VASP) and exclusively investigated the potential of monolayer Sb [44] for LIB anodes in rechargeable batteries (see Figure 6a). They noticed that the Li adsorption energies on monolayer Sb vary from 1.70 to 1.91 eV with a charge transfer of ~0.85 |e|, indicating the adsorption is relatively strong, as shown in Figure 6b,c. It is interesting to note that the semi-metallic monolayer Sb exhibits a semiconductor to metal transition (see Figure 6d) upon Li intercalation, accompanied by significant electron transfer from Li to Sb, consistent with earlier reports on different 2D materials [51]. The study also investigated the diffusion barrier of Li atoms on the surface of monolayer Sb and observed fast diffusion with a low energy barrier of 0.20 eV. This observed diffusion barrier is much lower compared to the bulk antimony electrode, which has a diffusion barrier of 1.73 eV. Since the volume expansion upon intercalation is one of the important

parameters to analyze the performance of electrode material, they also studied the volume expansion of monolayer Sb upon Li interaction and observed a structural deformation of $\sim 15\%$. Although this volume expansion is much less compared to the Sb metal, which is 135%, the possible alternatives for Sb-based anodes are highly demanding.

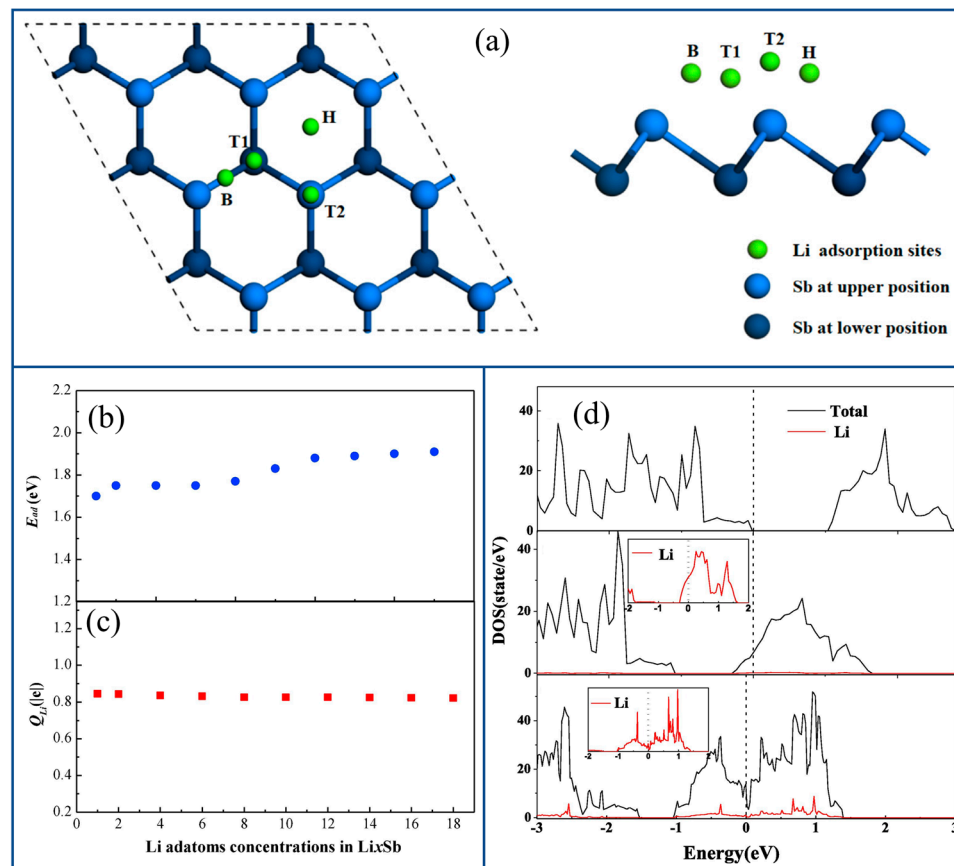


Figure 6. (a) Schematic illustration of the top and side geometries of 2D antimonene along with the possible Li adsorption sites. (b) Li adsorption energies and (c) amount of Bader charge transfer as a function of Li concentration in Li_xSb . (d) The density of states pristine antimonene (top panel), with single Li adsorption (middle panel), and T1–location (bottom panel). The black and red solid lines represent the total density of states (DOS) of Li adsorbed Sb and partial DOS of Li alone, respectively. The vertical black dashed vertical line indicates the Fermi level and is set as 0 eV. (Reproduced with permission from Ref. [51]. Copyright 2018, Elsevier).

The relatively high volume expansion of the monolayer Sb motivated the study of monolayer Sb-based heterostructures. In 2019, Wang et al. theoretically investigated the possibilities of constructing graphene/antimonene (G/Sb) heterostructures and reported their promising applications in high-cycle-capability anodes for fast-charging LIBs [46]. Their study revealed that G/Sb heterostructures possess a lower diffusion barrier, as shown in Figure 7a. Additionally, the charge/discharge performance of G/Sb is superior and has a volume expansion of 1%, which is much less compared to the Sb monolayer (15%) and bilayer (-6%). Although the G/Sb heterostructure has a minute bandgap of 0.06 eV, the partial density of states analysis revealed its metallic character with the presence of Li adatom and that the contributions at the Fermi level are mainly aroused due to the presence of p orbitals of Sb atoms, as shown in Figure 7b.

In addition to these studies, Wu et al. also reported the LIB applications of G/Sb heterostructures and reported a high mechanical strength, suitable for minimizing the volume expansion [52]. In addition to this, an improved electrical conductivity of G/Sb heterostructures when compared to antimonene has also been reported. Their simulation

pointed out that Li adatoms tried to occupy the interlayer region of G/Sb rather than the outer surfaces. Their study observed an improved theoretical capacity of G/Sb heterostructures (369 mAh g^{-1}), higher than that of monolayer Sb, but much less compared to many 2D materials. However, one can anticipate that the doping of carbon atoms, as well as the creation of heterostructures using carbon-based nanostructures, can help to improve the theoretical capacity as well as minimize the volume expansion of monolayer and bulk Sb-based electrodes, which is vital for the rational design of high-performance electrode materials for rechargeable LIBs.

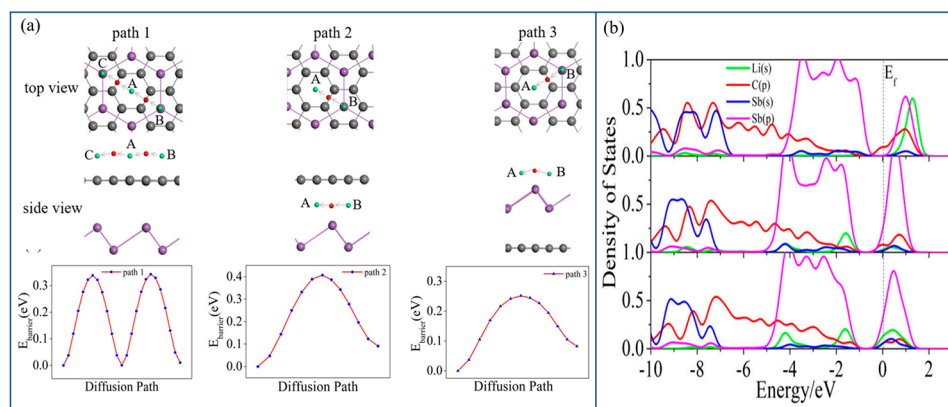


Figure 7. Top and side view of diffusion paths and corresponding energy profile of Li during the intercalation in G/Sb heterostructure. **(b)** Partial density of states analysis during the Li intercalation in G/Sb heterostructure with Li at different locations, consistent with **(a)**, Li/G/Sb (top panel), G/Li/Sb (middle panel), and G/Sb/Li (bottom panel). The vertical dashed line denotes the Fermi level and states at the Fermi level is mainly aroused from the p orbitals of Sb atoms. (Reproduced with permission from Ref. [52]. Copyright 2019, Elsevier).

5. Conclusions and Future Outlooks

To improve the lithium-ion battery performance, the conversion type of anodes is believed to be the right candidate. Among these candidates, Sb has one of the least volumetric changes during the lithium storage and possesses high volumetric properties comparable to the highly unstable silicon anodes. In addition, Sb-based batteries offer better safety features owing to their lower thermal runaway properties. This makes Sb a suitable candidate to replace graphite anodes. To meet the requirements of the market, the cyclic life of Sb has to be improved further. Hence, current research focuses on the problems existing on antimony anodes from single directional approaches such as micro-/nanostructuring or making composites. There should be more focus on multidimensional approaches to solve the existing problems in Sb anodes. Additionally, more studies should be reported on the underlying mechanism of charge and discharge mechanism which could be important in systematically manipulating the Sb anode properties. Research which focused on DFT studies also showed the potential of monolayer Sb for LIB anodes in rechargeable batteries, which could provide relatively strong Li adsorption. In conclusion, antimony is a rare element on the planet, but it offers intriguing features when it comes to the needs of energy storage systems. It possesses great volumetric capacities and, more crucially, good characteristics that make it suitable for use in considerably safer batteries. To take advantage of its qualities, more focus must be placed on recovering antimony from used anodes in order to make the most efficient use of available resources. The lack of literature on the recovery of Sb from used anodes is concerning and should be investigated further.

Author Contributions: All the authors contributed to data collection, writing the manuscript, obtaining necessary permissions and editing the final draft. All authors have read and agreed to the published version of the manuscript.

Funding: This research received no external funding.

Institutional Review Board Statement: Not applicable.

Informed Consent Statement: Not applicable.

Data Availability Statement: Not applicable.

Acknowledgments: SM acknowledge Deepthi Panoth for her valuable suggestions in improving the quality of this manuscript.

Conflicts of Interest: The authors declare no conflict of interest.

References

1. Nitta, N.; Wu, F.; Lee, J.T.; Yushin, G. Li-ion battery materials: Present and future. *Mater. Today* **2015**, *18*, 252–264. [[CrossRef](#)]
2. Chen, Y.; Kang, Y.; Zhao, Y.; Wang, L.; Liu, J.; Li, Y.; Liang, Z.; He, X.; Li, X.; Tavajohi, N.; et al. A review of lithium-ion battery safety concerns: The issues, strategies, and testing standards. *J. Energy Chem.* **2021**, *59*, 83–99. [[CrossRef](#)]
3. Sreejesh, M.; Shenoy, S.; Sridharan, K.; Kufian, D.; Arof, A.K.; Nagaraja, H.S. Melt quenched vanadium oxide embedded in graphene oxide sheets as composite electrodes for amperometric dopamine sensing and lithium ion battery applications. *Appl. Surf. Sci.* **2017**, *410*, 336–343. [[CrossRef](#)]
4. Asenbauer, J.; Eisenmann, T.; Kuenzel, M.; Kazzazi, A.; Chen, Z.; Bresser, D. The success story of graphite as a lithium-ion anode material—fundamentals, remaining challenges, and recent developments including silicon (oxide) composites. *Sustain. Energy Fuels* **2020**, *4*, 5387–5416. [[CrossRef](#)]
5. Zhang, W.-J. A review of the electrochemical performance of alloy anodes for lithium-ion batteries. *J. Power Sources* **2011**, *196*, 13–24. [[CrossRef](#)]
6. Chen, Y.; Li, X.; Zhou, L.; Mai, Y.-W.; Huang, H. Chapter 21—High-performance electrospun nanostructured composite fiber anodes for lithium-ion batteries. In *Multifunctionality of Polymer Composites*; Friedrich, K., Breuer, U., Eds.; William Andrew Publishing: Oxford, UK, 2015; pp. 662–689.
7. Li, H.; Yamaguchi, T.; Matsumoto, S.; Hoshikawa, H.; Kumagai, T.; Okamoto, N.L.; Ichitsubo, T. Circumventing huge volume strain in alloy anodes of lithium batteries. *Nat. Commun.* **2020**, *11*, 1584. [[CrossRef](#)]
8. He, J.; Wei, Y.; Zhai, T.; Li, H. Antimony-based materials as promising anodes for rechargeable lithium-ion and sodium-ion batteries. *Mater. Chem. Front.* **2018**, *2*, 437–455. [[CrossRef](#)]
9. Broussely, M.; Herreyre, S.; Biensan, P.; Kasztejna, P.; Nechev, K.; Staniewicz, R.J. Aging mechanism in Li ion cells and calendar life predictions. *J. Power Sources* **2001**, *97–98*, 13–21. [[CrossRef](#)]
10. Winter, M.; Besenhard, J.O.; Spahr, M.E.; Novák, P. Insertion Electrode Materials for Rechargeable Lithium Batteries. *Adv. Mater.* **1998**, *10*, 725–763. [[CrossRef](#)]
11. Saubanière, M.; Ben Yahia, M.; Lemoigno, F.; Doublet, M.-L. Influence of polymorphism on the electrochemical behavior of MxSb negative electrodes in Li/Na batteries. *J. Power Sources* **2015**, *280*, 695–702. [[CrossRef](#)]
12. Sangster, J.; Pelton, A.D. The Li-Sb (Lithium-Antimony) System. *J. Phase Equilibria* **1993**, *14*, 514–517. [[CrossRef](#)]
13. Darwiche, A.; Marino, C.; Sougrati, M.T.; Fraisse, B.; Stievano, L.; Monconduit, L. Better Cycling Performances of Bulk Sb in Na-Ion Batteries Compared to Li-Ion Systems: An Unexpected Electrochemical Mechanism. *J. Am. Chem. Soc.* **2012**, *134*, 20805–20811. [[CrossRef](#)] [[PubMed](#)]
14. Chang, D.; Huo, H.; Johnston, K.E.; Ménétrier, M.; Monconduit, L.; Grey, C.P.; Van der Ven, A. Elucidating the origins of phase transformation hysteresis during electrochemical cycling of Li-Sb electrodes. *J. Mater. Chem. A* **2015**, *3*, 18928–18943. [[CrossRef](#)]
15. Chen, B.; Liang, M.; Wu, Q.; Zhu, S.; Zhao, N.; He, C. Recent Developments of Antimony-Based Anodes for Sodium- and Potassium-Ion Batteries. *Trans. Tianjin Univ.* **2022**, *28*, 6–32. [[CrossRef](#)]
16. Rodriguez, J.R.; Hamann, H.J.; Mitchell, G.M.; Ortalan, V.; Pol, V.G.; Ramachandran, P.V. Three-Dimensional Antimony Nanochains for Lithium-Ion Storage. *ACS Appl. Nano Mater.* **2019**, *2*, 5351–5355. [[CrossRef](#)]
17. Hou, H.; Jing, M.; Yang, Y.; Zhu, Y.; Fang, L.; Song, W.; Pan, C.; Yang, X.; Ji, X. Sodium/Lithium Storage Behavior of Antimony Hollow Nanospheres for Rechargeable Batteries. *ACS Appl. Mater. Interfaces* **2014**, *6*, 16189–16196. [[CrossRef](#)]
18. Boebinger, M.G.; Yarema, O.; Yarema, M.; Unocic, K.A.; Unocic, R.R.; Wood, V.; McDowell, M.T. Spontaneous and reversible hollowing of alloy anode nanocrystals for stable battery cycling. *Nat. Nanotechnol.* **2020**, *15*, 475–481. [[CrossRef](#)]
19. Wang, S.; Lee, P.-K.; Yang, X.; Rogach, A.L.; Armstrong, A.R.; Yu, D.Y.W. Polyimide-cellulose interaction in Sb anode enables fast charging lithium-ion battery application. *Mater. Today Energy* **2018**, *9*, 295–302. [[CrossRef](#)]
20. Yi, Z.; Han, Q.; Zan, P.; Wu, Y.; Cheng, Y.; Wang, L. Sb nanoparticles encapsulated into porous carbon matrixes for high-performance lithium-ion battery anodes. *J. Power Sources* **2016**, *331*, 16–21. [[CrossRef](#)]
21. Wang, H.; Wu, X.; Qi, X.; Zhao, W.; Ju, Z. Sb nanoparticles encapsulated in 3D porous carbon as anode material for lithium-ion and potassium-ion batteries. *Mater. Res. Bull.* **2018**, *103*, 32–37. [[CrossRef](#)]
22. Ramireddy, T.; Rahman, M.M.; Xing, T.; Chen, Y.; Glushenkov, A.M. Stable anode performance of an Sb-carbon nanocomposite in lithium-ion batteries and the effect of ball milling mode in the course of its preparation. *J. Mater. Chem. A* **2014**, *2*, 4282. [[CrossRef](#)]

23. Dashairya, L.; Das, D.; Saha, P. Electrophoretic deposition of antimony/reduced graphite oxide hybrid nanostructure: A stable anode for lithium-ion batteries. *Mater. Today Commun.* **2020**, *24*, 101189. [[CrossRef](#)]
24. Zhang, X.; Lai, F.; Chen, Z.; He, X.; Li, Q.; Wang, H. Metallic Sb nanoparticles embedded in carbon nanosheets as anode material for lithium ion batteries with superior rate capability and long cycling stability. *Electrochim. Acta* **2018**, *283*, 1689–1694. [[CrossRef](#)]
25. Lv, H.; Qiu, S.; Lu, G.; Fu, Y.; Li, X.; Hu, C.; Liu, J. Nanostructured Antimony/carbon Composite Fibers as Anode Material for Lithium-ion Battery. *Electrochim. Acta* **2015**, *151*, 214–221. [[CrossRef](#)]
26. Cheng, Y.; Yi, Z.; Wang, C.; Wang, L.; Wu, Y.; Wang, L. Nanostructured Carbon/Antimony Composites as Anode Materials for Lithium-Ion Batteries with Long Life. *Chem.—Asian J.* **2016**, *11*, 2173–2180. [[CrossRef](#)]
27. Wu, Y.; Pan, Q.; Zheng, F.; Ou, X.; Yang, C.; Xiong, X.; Liu, M.; Hu, D.; Huang, C. Sb@C/expanded graphite as high-performance anode material for lithium ion batteries. *J. Alloys Compd.* **2018**, *744*, 481. [[CrossRef](#)]
28. Chang, C.-C. Sb-coated mesophase graphite powder as anode material for lithium-ion batteries. *J. Power Sources* **2008**, *175*, 874–880. [[CrossRef](#)]
29. Chen, W.X.; Lee, J.Y.; Liu, Z. The nanocomposites of carbon nanotube with Sb and SnSb_{0.5} as Li-ion battery anodes. *Carbon* **2003**, *41*, 959–966. [[CrossRef](#)]
30. Yi, Z.; Han, Q.; Ju, S.; Wu, Y.; Cheng, Y.; Wang, L. Fabrication of One-Dimensional Sb@TiO₂ Composites as Anode Materials for Lithium-Ion Batteries. *J. Electrochem. Soc.* **2016**, *163*, A2641–A2646. [[CrossRef](#)]
31. Yu, J.; Meng, B.; Fu, Y.; Huang, W.; Wang, L.; Wang, Q.; Li, L. Strongly binding natural stibnite on carbon fiber as anode for lithium-ion batteries. *Ionics* **2020**, *26*, 5915–5922. [[CrossRef](#)]
32. Huang, Y.; Ji, C.; Pan, Q.; Zhang, X.; Zhang, J.; Wang, H.; Liao, T.; Li, Q. Scalable synthesis of Sb/MoS₂/C composite as high performance anode material for lithium ion batteries. *J. Alloys Compd.* **2017**, *728*, 1139–1145. [[CrossRef](#)]
33. Wang, B.; Xia, Y.; Deng, Z.; Zhang, Y.; Wu, H. Three-dimensional cross-linked MnO/Sb hybrid nanowires co-embedded nitrogen-doped carbon tubes as high-performance anode materials for lithium-ion batteries. *J. Alloys Compd.* **2020**, *835*, 155239. [[CrossRef](#)]
34. Bian, X.; Dong, Y.; Zhao, D.; Ma, X.; Qiu, M.; Xu, J.; Jiao, L.; Cheng, F.; Zhang, N. Microsized Antimony as a Stable Anode in Fluoroethylene Carbonate Containing Electrolytes for Rechargeable Lithium-/Sodium-Ion Batteries. *ACS Appl. Mater. Interfaces* **2020**, *12*, 3554–3562. [[CrossRef](#)] [[PubMed](#)]
35. Liu, X.; Tian, Y.; Cao, X.; Li, X.; Le, Z.; Zhang, D.; Li, X.; Nie, P.; Li, H. Aerosol-Assisted Synthesis of Spherical Sb/C Composites as Advanced Anodes for Lithium Ion and Sodium Ion Batteries. *ACS Appl. Energy Mater.* **2018**, *1*, 6381–6387. [[CrossRef](#)]
36. Zhou, X.; Ding, J.; Lu, H.; Qi, Z.; Yan, C. Controllable synthesis of Sb/reduced graphene oxide nanocomposite by oxygen-containing groups for ultra-stable lithium/sodium storage. *Mater. Chem. Phys.* **2021**, *270*, 124873. [[CrossRef](#)]
37. Tian, J.; Yang, H.; Fu, C.; Sun, M.; Wang, L.; Liu, T. In-situ synthesis of microspherical Sb@C composite anode with high tap density for lithium/sodium-ion batteries. *Compos. Commun.* **2020**, *17*, 177–181. [[CrossRef](#)]
38. Kumari, P.; Sharma, K.; Pal, P.; Kumar, M.; Ichikawa, T.; Jain, A. Highly efficient & stable Bi & Sb anodes using lithium borohydride as solid electrolyte in Li-ion batteries. *RSC Adv.* **2019**, *9*, 13077–13081. [[CrossRef](#)]
39. Schulze, M.C.; Belson, R.M.; Kraynak, L.A.; Prieto, A.L. Electrodeposition of Sb/CNT composite films as anodes for Li- and Na-ion batteries. *Energy Storage Mater.* **2020**, *25*, 572–584. [[CrossRef](#)]
40. Yin, W.; Chai, W.; Wang, K.; Ye, W.; Rui, Y.; Tang, B. Facile synthesis of Sb nanoparticles anchored on reduced graphene oxides as excellent anode materials for lithium-ion batteries. *J. Alloys Compd.* **2019**, *797*, 1249–1257. [[CrossRef](#)]
41. Feng, P.; Cui, Z.; He, S.-A.; Liu, Q.; Zhu, J.; Xu, C.; Zou, R.; Hu, J. Reversible formation of networked porous Sb nanoparticles during cycling: Sb nanoparticles encapsulated in a nitrogen-doped carbon matrix with nanorod structures for high-performance Li-ion batteries. *J. Mater. Chem. A* **2019**, *7*, 24292–24300. [[CrossRef](#)]
42. Le, H.T.T.; Pham, X.-M.; Park, C.-J. Facile citrate gel synthesis of an antimony-carbon nanosponge with enhanced lithium storage. *New J. Chem.* **2019**, *43*, 10716–10725. [[CrossRef](#)]
43. Gao, Y.; Tian, W.; Huo, C.; Zhang, K.; Guo, S.; Zhang, S.; Song, X.; Jiang, L.; Huo, K.; Zeng, H. Tailoring natural layered β -phase antimony into few layer antimonene for Li storage with high rate capabilities. *J. Mater. Chem. A* **2019**, *7*, 3238–3243. [[CrossRef](#)]
44. Wang, W.; Xu, J.; Xu, Z.; Zheng, W.; Wang, Y.; Jia, Y.; Ma, J.; Wang, C.; Xie, W. Ultrafine antimony (Sb) nanoparticles encapsulated into a carbon microfiber framework as an excellent LIB anode with a superlong life of more than 5000 cycles. *Nanotechnology* **2020**, *31*, 215403. [[CrossRef](#)] [[PubMed](#)]
45. Meng, W.; Guo, M.; Chen, J.; Li, D.; Wang, Z.; Yang, F. Porous Sb with three-dimensional Sb nanodendrites as electrode material for high-performance Li/Na-ion batteries. *Nanotechnology* **2020**, *31*, 175401. [[CrossRef](#)]
46. Ning, X.; Zhou, X.; Luo, J.; Ma, L.; Zhan, L. Ion-assisted construction of Sb/N-doped graphene as an anode for Li/Na ion batteries. *Nanotechnology* **2019**, *31*, 095404. [[CrossRef](#)]
47. Dashairya, L.; Das, D.; Saha, P. Binder-free electrophoretic deposition of Sb/rGO on Cu foil for superior electrochemical performance in Li-ion and Na-ion batteries. *Electrochim. Acta* **2020**, *358*, 136948. [[CrossRef](#)]
48. Wang, N.; Bai, Z.; Qian, Y.; Yang, J. Double-Walled Sb@TiO_{2-x} Nanotubes as a Superior High-Rate and Ultralong-Lifespan Anode Material for Na-Ion and Li-Ion Batteries. *Adv. Mater.* **2016**, *28*, 4126–4133. [[CrossRef](#)]
49. Yu, L.; Zhang, L.; Fu, J.; Yun, J.; Kim, K.H. Hierarchical Tiny-Sb encapsulated in MOFs derived-carbon and TiO₂ hollow nanotubes for enhanced Li/Na-Ion half-and full-cell batteries. *Chem. Eng. J.* **2021**, *417*, 129106. [[CrossRef](#)]

50. Allcorn, E.; Manthiram, A. Thermal Stability of Sb and Cu₂Sb Anodes in Lithium-Ion Batteries. *J. Electrochem. Soc.* **2015**, *162*, A1778–A1786. [[CrossRef](#)]
51. Su, J.; Duan, T.; Li, W.; Xiao, B.; Zhou, G.; Pei, Y.; Wang, X. A first-principles study of 2D antimonene electrodes for Li ion storage. *Appl. Surf. Sci.* **2018**, *462*, 270–275. [[CrossRef](#)]
52. Wang, X.; Tang, C.; Zhou, X.; Zhu, W.; Cheng, C. Theoretical investigating of graphene/antimonene heterostructure as a promising high cycle capability anodes for fast-charging lithium ion batteries. *Appl. Surf. Sci.* **2019**, *491*, 451–459. [[CrossRef](#)]